

State-dependent receptive-field restructuring in the visual cortex

Florentin Wörgötter, Katrin Suder, Yongqiang Zhao, Nicolas Kerscher, Ulf T. Eysel & Klaus Funke

Institut für Physiologie, Ruhr-Universität Bochum, D-44780 Bochum, Germany

To extract important information from the environment on a useful timescale, the visual system must be able to adapt rapidly to constantly changing scenes. This requires dynamic control of visual resolution, possibly at the level of the responses of single neurons. Individual cells in the visual cortex respond to light stimuli on particular locations (receptive fields) on the retina, and the structure of these receptive fields can change in different contexts¹⁻⁴. Here we show experimentally that the shape of receptive fields in the primary visual cortex of anaesthetized cats undergoes significant modifications, which are correlated with the general state of the brain as assessed by electroencephalography: receptive fields are wider during synchronized states and smaller during non-synchronized states. We also show that cortical receptive fields shrink over time when stimulated with flashing light spots. Finally, by using a network model we account for the changing size of the cortical receptive fields by dynamically rescaling the levels of excitation and inhibition in the visual thalamus and cortex. The observed dynamic changes in the sizes of the cortical receptive field could be a reflection of a process that

adapts the spatial resolution within the primary visual pathway to different states of excitability.

The frequency content of the electroencephalogram (EEG) is correlated to behavioural states. In a drowsy state, α -waves and some δ -waves predominate, whereas mainly β -waves are observed during attentive perception. This indicates that the temporal and spatial resolution of the visual system might also change in a way that is correlated with EEG frequency content. Indeed, the temporal characteristics of the cell responses in the visual thalamus (lateral geniculate nucleus, LGN) are markedly EEG-correlated. Brief stereotyped bursts of LGN neurons are seen during an α/δ -wave-dominated EEG (a synchronized EEG)^{5,6}, whereas the cells fire in a tonic, long-lasting way during a β -wave-dominated EEG (a non-synchronized EEG⁶⁻⁹).

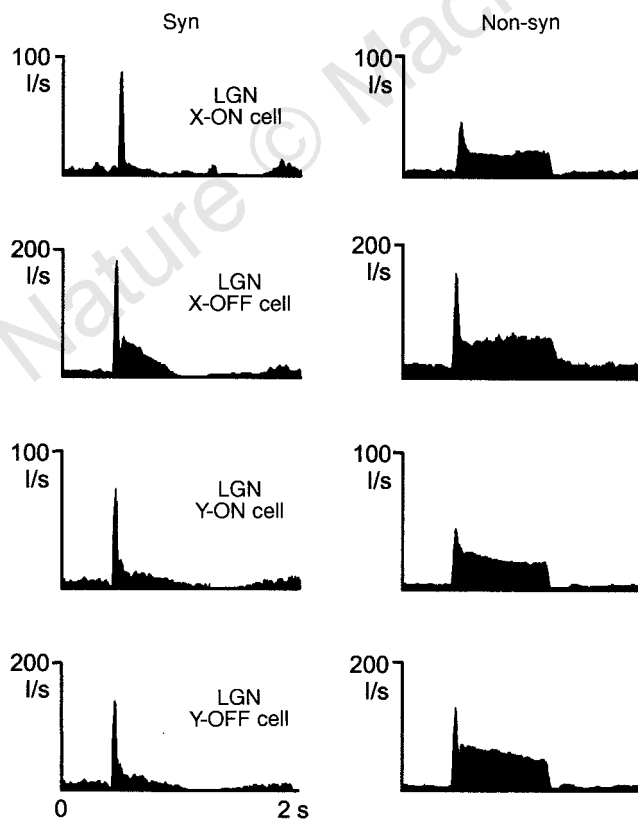


Figure 1 Temporal characteristics of LGN responses to flashing light spots (peristimulus time histograms) during different EEG states. Cells respond more tonically during non-synchronized EEG but more phasically during synchronized EEG. I/s, impulses per second. X and Y cells are different cell classes in the LGN.

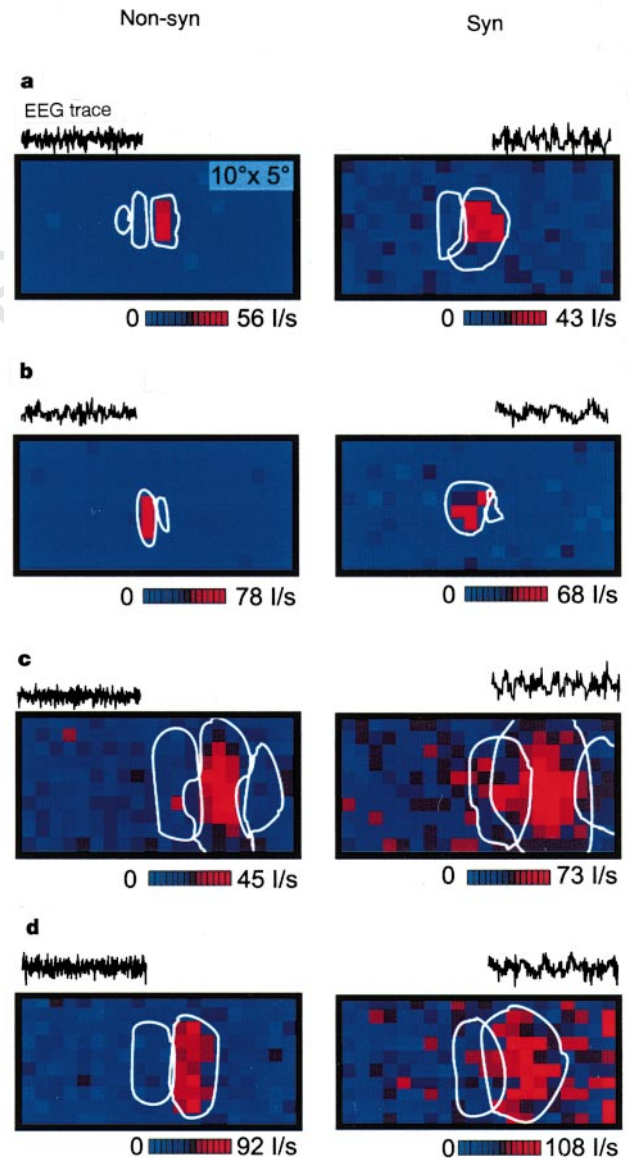


Figure 2 Changing shape of cortical receptive fields during different EEG states. The impulse rate of a single subfield is colour-coded according to the scales shown (maximum scaling) and the complete receptive field is outlined in white. Parts (5 s) from the corresponding EEG traces are shown. Receptive fields are wider during synchronized EEG and the subfield overlap increases. **a**, End-stopped simple cell 'Off' response; **b**, end-stopped simple cell 'On' response; **c**, simple cell 'Off' response; **d**, simple cell 'On' response. (End-stopped means that these cells are inhibited ('stopped') by stimuli which extend beyond the long-'ends' of their receptive field.)

The peristimulus time histograms (PSTHs) shown in Fig. 1 were obtained from study of four LGN cells (total $n = 55$) during synchronized (left) and non-synchronized (right) EEG states. A strong and long-lasting tonic response component is visible only in the right-hand PSTHs. During synchronized EEG, however, the tonic responses are strongly diminished, whereas the phasic peaks have a high amplitude.

Neurons in the visual cortex are the main targets of LGN neurons. Therefore, one would expect that these two different temporal activity patterns of LGN cells should also have an effect on cortical cell behaviour. Figure 2 shows four representative receptive-field maps from a sample of 63 cortical cells recorded during the same EEG states as the PSTHs. Maps were obtained from cell responses, elicited with flashing bright and dark dot stimuli on a grid that covers the receptive field completely ('reverse-correlation method', flash duration 300 ms; this stimulus duration induces phasic and tonic LGN activity^{10,11}). Examples of individual 'On' or 'Off' subfields of simple cells are shown, recorded at different retinal eccentricities. The receptive field of each cell is substantially wider during a synchronized EEG (such that the subfield overlap increases) than during a non-synchronized EEG. The almost identical activity levels in the corresponding diagram pairs in Fig. 2 indicate that the observed receptive-field changes cannot be attributed merely to variations in overall activity which does not seem to be correlated to the EEG, as seen from the scale bars.

We determined quantitatively the degree of synchronization in the EEG and its correlation to the receptive-field size. The scatter plot in Fig. 3 shows that cortical receptive fields become significantly wider during synchronized EEG states. The receptive fields grow, on average, by 27% during an average 2.5-fold power increase in the δ -range (1–4 Hz). All cells were pooled, because very similar effects were found for simple ($n = 53$) and complex ($n = 10$) cells throughout all recording depths.

Another characteristic feature can be seen in the PSTHs in Fig. 1: the tonic response in an LGN cell during non-synchronized EEG is always preceded by a short phasic peak. We therefore predict that, during a non-synchronized EEG, a transition from a wider to a smaller receptive field should occur, in parallel with the transition from the phasic to the tonic part of the LGN response. We demonstrate this effect in Fig. 4, in which the width of the receptive

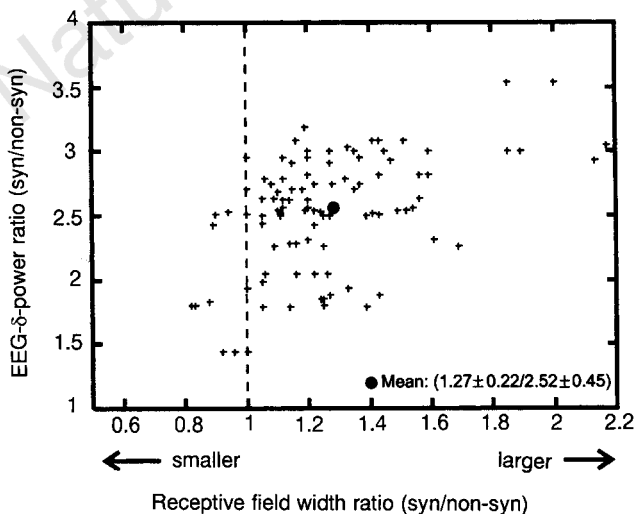


Figure 3 Scatter plot of EEG state versus subfield width for 97 subfields. The ratio of subfield width during synchronized EEG divided by that during non-synchronized EEG is plotted on the x-axis. The ratio of the power in the δ -range (1–4 Hz) for the same two recordings is plotted on the y-axis. The coordinate 1.0 indicates no change of the corresponding variable. Most samples (84 of 97) exhibit an increase in subfield size during increasingly synchronized EEG states.

field is plotted against the time from stimulus onset to response of the cell (latency) for four more example cells. A fast, nonlinear shrinkage is seen after the first 50 ms of the response. This corresponds directly with the duration of the phasic LGN response, which is about 50 ms long (see PSTHs in Fig. 1) and rules out the possibility that normal adaptation effects, which have a duration of much more than 100 ms, are responsible for this effect.

These results confirm that cortex cells in general respond more vigorously to transient stimuli. However, this affects not only the temporal structure of their response but also the spatial shape of their receptive fields (Fig. 4). The percentage temporal change of the subfield width, comparing the sizes after 70 ms (100% value) with those after 200 ms, follows a distribution with a mean subfield shrinkage of $22.2\% \pm 12.6\%$. The median is 23.1% and the distribution is only slightly skewed (skewness +0.99); thus, the deviation from a gaussian distribution is small. The distribution yielded 54 out of 97 subfields, which shrank by more than 20%.

In a model we addressed the issue of which mechanisms might underlie the observed effects. We propose that temporal restructuring of the thalamic and cortical network activity leads to the observed effects (Fig. 5). The visual part of the thalamic reticular nucleus (the perigeniculate nucleus, PGN) integrates brain-stem activity, which is involved in the control of the sleep-waking cycle¹²,

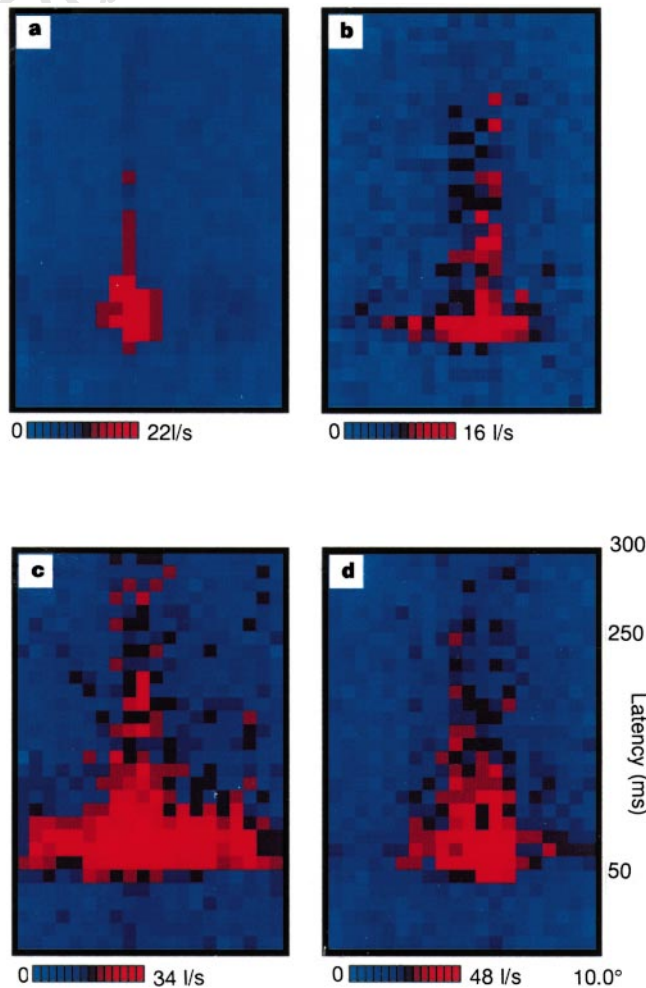


Figure 4 Shrinking of the receptive-field width for cortical cells as time after stimulation increases. Only the non-synchronized EEG state was studied. The data were analysed in successive windows of 10-ms duration. For every x-location in the cortical map, we collected the responses from all y-locations. **a**, End-stopped simple cell 'On' response; **b**, simple cell 'On' response; **c**, simple cell 'Off' response; **d**, complex cell 'On' response.

and thalamic relay cells are inhibited by cells of the PGN¹³. This inhibitory loop may be involved in the generation of different EEG waveforms such as sleep spindles¹⁴ and—together with the corticothalamic pathway—may act in the generation of synchronized δ -waves¹⁵.

The model indicates that a high level of inhibition of LGN neurons by PGN neurons during synchronized EEG may lead to bursting activity in the LGN, which, in turn, would result in wider and less specific cortical receptive fields. On the other hand, reduced LGN inhibition during non-synchronized EEG would drive the LGN cells into tonic transmission mode (often called 'single-spike mode'^{16,17}) and the cortical receptive fields would then be smaller (Fig. 5). Thus, the temporal structure of the thalamic activity could be a trigger that leads the subsequent intracortical interactions (for example, corticothalamic feedback and cortical lateral inhibition in the model) to react in a state-dependent way, resulting in the observed receptive-field restructuring.

The model predicts that cortical receptive fields should widen when the level of inhibition at the LGN cells is increased. This could be tested by, for example, microiontophoretic application of an excitatory transmitter in the PGN. The far-reaching PGN connec-

tions would inhibit a relatively large population of LGN cells, so that the predicted widening of receptive fields should be visible in the cortex.

Our experimental and modelling results indicate that a quite marked spatial restructuring of cortical receptive fields occurs during different EEG states, and that this effect could be due to the temporal structure of the thalamic cell (LGN and PGN) responses and the action of the corticothalamic and intracortical networks. These results indicate that temporal and spatial restructuring of visual cortical receptive fields may be important in controlling the resolution of visual processing in the primary visual pathway in a state-dependent way.

Methods

Experimental methods. Data were obtained from single-unit recordings, using glass pipettes in area 17 of four cats (63 cells total). Animals were first anaesthetized with ketamine. Surgery was performed to enable infusion of alcuronium chloride, Ringer solution and glucose through the femor artery and artificial respiration through the trachea (N₂O : O₂ = 70 : 30, 0.4% halothane) and to allow access to area 17. An additional craniotomy was made above area 18 to insert a 0.5-mm-diameter silver ball electrode epidurally for EEG recording. Blood pressure (>90 mm Hg) and end-expired CO₂ (\approx 3.8%) were held within physiological limits. Cells were stimulated with small dots (0.5 \times 0.5 degrees, \pm 50% contrast to background) on a computer screen. The screen was centred on the receptive field and rotated to the preferred orientation of the cell. The dot was presented about 200 times at every grid location in the diagram for 300 ms at each location (total recording time for a single cell >4 h). All spikes were counted in a window of 300-ms duration after a latency of 50 ms following every repeated stimulus presentation (reverse-correlation technique^{10,11}). See refs 18, 19 for more details.

Data analysis. We measured the relative power in the δ -range (1–4 Hz) with respect to the total power, up to 30 Hz¹⁸. A relative power in the δ -range of >70% was taken to represent highly synchronized EEG, and a relative power of <30% was taken to represent non-synchronized EEG; the middle range was not used. Finally, spike data were sorted with respect to these two ranges for presentation in the diagrams and statistical treatment. To determine the subfield width of a receptive field for every x -location in the map, we collected the responses from all y -locations. We then used the half-width at half-height, measured across the resulting peak, to characterize the width of a subfield.

Modelling. The model is restricted to a single 'On' subfield. Multiple antagonistic subfields can be generated by repeating the shown module. The same flashing stimulus as that used in the experiments was stimulated. Single model cells represented leaky 'integrate-and-fire' type neurons. LGN cells can switch between a depolarized, tonic transmission mode (maximum impulse rate \sim 250 Hz, contrast-dependent) and a hyperpolarized, phasic burst mode (2–8 spikes with interspike intervals of <2.5 ms, not contrast-dependent). To switch to the burst mode, PGN activity is increased; which is a major source of inhibition at the LGN cells^{20,21}. A PGN activity of 10 (or 25) spikes per second was used to mimic a non-synchronized (or synchronized) EEG state. Firing frequencies of PGN and LGN cells are approximately antagonistic¹⁹. We added synaptic noise at all stages. We simulated 4,000 cells on two two-dimensional grids (LGN/PGN and cortex) arranged topographically. Excitatory feed-forward connections are strong, whereas the corticothalamic feedback is weak and cannot drive the LGN cells on its own. The more tonically driven corticothalamic feedback enhances the depolarization level in the LGN only during non-synchronized EEG.

Received 20 July; accepted 22 September 1998.

1. Knierim, J. J. & van Essen, D. C. Neuronal responses to static texture patterns in area V1 of the alert macaque monkey. *J. Neurophysiol.* **67**, 961–980 (1992).
2. Sillito, A. M., Grieve, K. L., Jones, H. E., Cudeiro, J. & Davis, J. Visual cortical mechanisms detecting focal orientation discontinuities. *Nature* **378**, 492–496 (1995).
3. Zipser, K., Lamme, V. A. & Schiller, P. H. Contextual modulation in primary visual cortex. *J. Neurosci.* **16**, 7376–7389 (1996).
4. Gilbert, C. D. Adult cortical dynamics. *Physiol. Rev.* **78**, 467–485 (1998).
5. Steriade, M., McCormick, D. A. & Sejnowski, T. J. Thalamocortical oscillations in the sleeping and aroused brain. *Science* **262**, 679–685 (1993).
6. McCarley, R. W., Benoit, O. & Barrionuevo, G. Lateral geniculate nucleus unitary discharge in sleep and waking: state- and rate-specific aspects. *J. Neurophysiol.* **50**, 7980–818 (1983).
7. Funke, K. & Eysel, U. T. EEG-dependent modulation of response dynamic of cat dLGN relay cells and the contribution of the corticogeniculate feedback. *Brain Res.* **573**, 217–227 (1992).

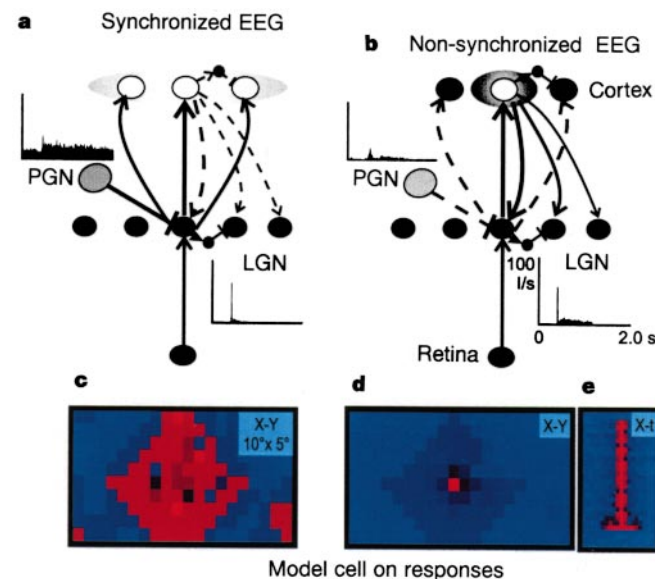


Figure 5 Model of the primary visual pathway during a synchronized and a non-synchronized EEG, and receptive-field maps for the corresponding states. **a**, Synchronized EEG; **b**, non-synchronized EEG; **c–e**, receptive-field maps. **a**, **b**, Insets show the activity of real LGN and PGN cells¹⁹. Anatomical connections²² are identical in both situations; different line thicknesses and types indicate only the effective connectivity²³, which changes in a state-dependent way. **a**, During synchronized EEG, inhibition of LGN neurons by PGN neurons is strong. LGN cells are, therefore, hyperpolarized⁵ and fire in phasic burst mode^{16,17}. The bursts of LGN activity are transmitted to the cortex. Because of the high firing frequency in a burst, strong temporal summation occurs at the target cells, and even those targets that receive weaker synapses (lateral to the main target cell group) become superthreshold. Wide cortical receptive fields are obtained. **b**, During non-synchronized EEG, inhibition by PGN neurons is weak. LGN cells are, therefore, depolarized⁵ and fire in tonic transmission mode^{16,17}. The lower firing frequencies in the sustained LGN activity result in a less marked temporal summation at their cortical targets and only cortical cells with strong synapses become activated (centre). This leads to the production of small cortical receptive fields. The prolonged cortical activity drives intracortical lateral inhibition and corticothalamic feedback. The excitatory feedback helps to keep the LGN cells in tonic transmission mode, while intracortical lateral inhibition further sharpens the cortical receptive field. **c**, Receptive field during a synchronized EEG state. **d**, Receptive field during a non-synchronized EEG state. **e**, Shrinking of the receptive-field width as time after stimulus increases. t , time.

8. Sawai, H., Morigiwa, K. & Fukuda, Y. Effects of EEG synchronization on visual responses of cat's lateral geniculate relay cells: a comparison among Y, X and W cells. *Brain Res.* **455**, 394–400 (1988).
9. Lo, F. S., Lu, S. M. & Sherman, S. M. Intracellular and extracellular *in vivo* recording of different response modes for relay cells of the cat's lateral geniculate nucleus. *Exp. Brain Res.* **83**, 317–328 (1991).
10. DeAngelis, G. C., Ohzawa, I. & Freeman, R. D. Spatiotemporal organization of simple-cell receptive fields in the cats striate cortex. I. General characteristics and postnatal development. *J. Neurophysiol.* **69**, 1091–1117 (1993).
11. Eckhorn, R., Krause, F. & Nelson, J. J. The RF-cinematogram—a cross-correlation technique for mapping several visual receptive fields at once. *Biol. Cybern.* **69**, 37–55 (1993).
12. Steriade, M. Arousal: revisiting the reticular activating system. *Science* **272**, 225–226 (1996).
13. Ahlsen, G., Lindstroem, S. & Lo, F.-S. Interaction between inhibitory pathways to principal cells in the lateral geniculate nucleus of the cat. *Exp. Brain Res.* **58**, 134–143 (1985).
14. Steriade, M., Domich, L., Oakson, G. & Deschenes, M. The deafferented reticular thalamic nucleus generates spindle rhythmicity. *J. Neurophysiol.* **57**, 260–273 (1987).
15. Timofeev, I. & Steriade, M. Low-frequency rhythms in the thalamus of intact-cortex and decorticated cats. *J. Neurophysiol.* **76**, 4152–4168 (1996).
16. Jahnsen, H. & Llinas, R. Electrophysiological properties of guinea-pig thalamic neurons: an *in vitro* study. *J. Physiol.* **349**, 205–226 (1984).
17. McCormick, D. A. & Pape, H. C. Properties of a hyperpolarization-activated cation current and its role in rhythmic oscillation in thalamic relay neurons. *J. Physiol.* **431**, 291–318 (1990).
18. Wörgötter, F., Nelle, E., Li, B. & Funke, K. The influence of corticothalamic feedback on the temporal structure of visual response of cat thalamic relay cells. *J. Physiol.* **509**, 797–815 (1998).
19. Funke, K. & Eysel, U. T. Inverse correlation of firing patterns of single topographically matched perigeniculate neurons and cat dorsal lateral geniculate relay cells. *Vis. Neurosci.* **15**, 711–729 (1998).
20. Ulrich, D. J., Cucchiari, J. B., Humphrey, A. L. & Sherman, S. M. Morphology and axonal projection patterns of individual neurons in the cat perigeniculate nucleus. *J. Neurophysiol.* **65**, 1528–1541 (1991).
21. Bal, T. & McCormick, D. A. Ionic mechanisms of rhythmic burst firing and tonic activity in the nucleus reticularis thalami, a mammalian pacemaker. *J. Physiol.* **468**, 669–691 (1993).
22. Sherman, S. M. & Guillery, R. W. Functional organization of thalamocortical relays. *J. Neurophysiol.* **76**, 1367–1395 (1996).
23. Aertsen, A. M. H. J., Gerstein, G. L., Habib, M. K. & Palm, G. Dynamics of neuronal firing correlation: modulation of "effective connectivity". *J. Neurophysiol.* **61**, 900–917 (1989).

Acknowledgements. We acknowledge the support of the DFG and the HFSP. We thank J. Macklis for suggestions on the manuscript.

Correspondence and requests for materials should be addressed to E.W. (e-mail: worgott@neurop.ruhr-uni-bochum.de).

The nuclear hormone receptor SEX-1 is an X-chromosome signal that determines nematode sex

Ilil Carmi*, Jennifer B. Kopczyński† & Barbara J. Meyer*

* Howard Hughes Medical Institute and Department of Molecular and Cell Biology, University of California, Berkeley, Berkeley, California 94720-3204, USA

Organisms in many phyla determine sexual fate by distinguishing one X chromosome from two. Here we use the model organism *Caenorhabditis elegans* to dissect such an X-chromosome-counting mechanism in molecular detail. In this nematode, several genes on the X chromosome called X signal elements communicate X-chromosome dose by controlling the activity of the sex-determination gene *xol-1* (refs 1, 2). *xol-1* specifies male (XO) fate when active and hermaphrodite (XX) fate when inactive^{3,4}. The only X signal element described so far represses *xol-1* post-transcriptionally, but *xol-1* is repressed in XX animals by transcriptional and post-transcriptional mechanisms². Here we identify a nuclear-hormone-receptor homologue, SEX-1, that regulates the transcription of *xol-1*. We show that *sex-1* is vital to X-chromosome counting: changing *sex-1* gene dose in XX or XO embryos causes sexual transformation and death from inadequate dosage compensation (the hermaphrodite-specific process that equalizes X-gene expression between the sexes⁵). The SEX-1 protein acts directly on *xol-1*, associating with its promoter *in vivo* and repressing *xol-1* transcription in XX embryos. Thus, *xol-1* is the direct molecular target of the primary sex-determination signal, and the dose of a nuclear hormone receptor helps to communicate X-chromosome number to determine nematode sex.

To understand how small quantitative differences in molecular

signals can be translated into alternative developmental fates, we searched for components of the primary sex-determination signal in *C. elegans*. We conducted a genetic screen designed to detect regulators of *xol-1* (Fig. 1a). In the screen we used a *xol-1::lacZ* reporter transgene (*yIs2*, Fig. 1b) that mimics the sex-specific response of the wild-type *xol-1* gene to the sex-determination signal, namely, high levels of activity in XO embryos and low levels in XX embryos⁴. We sought mutations that increased β -galactosidase activity in XX embryos, reasoning that such mutations might have reduced the X signal and thereby derepressed the endogenous *xol-1* gene. As *xol-1* also controls dosage compensation, derepression of *xol-1* in mutant XX animals causes death from increased X-gene expression⁴. Thus, to prevent hermaphrodite lethality from complicating the screen, we deleted *xol-1* from the parental strain. From 5,000 mutagenized haploid genomes, we identified two X-linked and 16 autosomal mutations. We show below that the X-linked mutation *y263* identifies an X-chromosome signal element, which we call *sex-1* (signal element on X).

As *yIs2* encodes a translational fusion, our screen had the potential to identify both transcriptional and post-transcriptional regulators of *xol-1*. To distinguish between these possibilities, we studied the effect of *sex-1* mutations on a transcriptional *Pxol-1::lacZ* fusion, *yIs33* (Fig. 1b). The original *sex-1* allele (*y263*), a second *sex-1* allele (*gm41*) obtained in an independent screen, and a chromosomal deficiency (*nDf19*) of the *sex-1* region all increased expression of *yIs33* in XX embryos, indicating that *sex-1* may be a transcriptional repressor of *xol-1* in hermaphrodites and that *sex-1* mutations reduce or eliminate its function (Fig. 1c–e). High *Pxol-1::lacZ* expression in *sex-1* XX mutants was seen only during

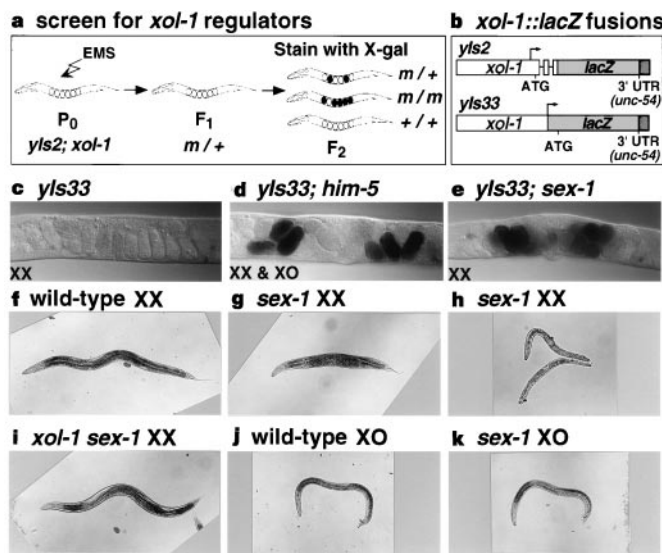


Figure 1 *sex-1* represses *xol-1* transcription in XX animals. **a**, The genetic screen used to identify regulators of *xol-1*, including *sex-1* (see Methods). *m* indicates a mutant gene. **b**, The integrated *xol-1::lacZ* translational¹ (*yIs2*) and *Pxol-1::lacZ* transcriptional² (*yIs33*) reporter transgenes. Arrows denote presumed start points of transcription. UTR, untranslated region. **c–e**, Nomarski photomicrographs of gravid *yIs33* hermaphrodites, fixed and stained with X-gal. **c**, Wild-type hermaphrodites produce only XX embryos, which express low levels of *lacZ*. **d**, *him-5* hermaphrodites produce ~33% XO embryos, which express high levels of *lacZ*, reflecting the XO-specific activation of *xol-1* transcription. **e**, *sex-1* mutations increase *lacZ* expression, suggesting that *sex-1* normally represses *xol-1* transcription in XX embryos. **f–k**, Photomicrographs of wild-type and *sex-1* mutant XX and XO animals. **f**, Wild-type hermaphrodite. **g, h**, The surviving *sex-1* XX mutants exhibit Dumpy and Egl phenotypes (**g**), which are characteristic of dosage-compensation defects, and masculinization (**h**), which is characteristic of sex-determination defects. **i**, *xol-1* mutations suppress all the *sex-1* mutant phenotypes. **j, k**, *sex-1* mutant males (**k**) are indistinguishable from wild-type males (**j**).

† Present address: Exelixis Pharmaceuticals, Inc., 260 Littlefield Avenue, South San Francisco, California 94080, USA